Princeton Plasma Physics Laboratory

Improving Confinement in Quasi-axisymmetric Stellarators

H.E. Mynick, A.H. Boozer, and L.P. Ku

June 2006

PPPL
PRINCETON PLASMA PHYSICS LABORATORY
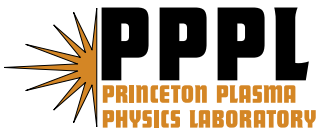
Princeton Plasma Physics Laboratory
Report Disclaimers

PPPL Report Availability

Improving confinement in quasi-axisymmetric stellarators

H.E. Mynick[a], A.H. Boozer[b] and L.P. Ku[a]

[a] *Princeton Plasma Physics Laboratory, Princeton, NJ 08543*

[b] *Dept. of Applied Physics & Applied Mathematics,*

Columbia University, New York, NY 10027

The confinement characteristics of some related quasi-axisymmetric stellarator designs are compared, to gain more physical understanding of what causes the differences in their transport. From this, some general rules are found for features of QA magnetic geometries which are deleterious or helpful for confinement.

In this work, we compare the confinement characteristics of 3 related quasi-axisymmetric (QA) stellarator designs, to better understand what causes the differences in their transport. From this, we distill some simple rules for features of the QA magnetic geometry which are deleterious or beneficial for confinement.

The National Compact Stellarator Experiment (NCSX)[1], now under construction, is designed to have low neoclassical transport of thermal particles, much smaller than expected levels from anomalous transport. Its confinement of energetic particles is, however, more problematic. For example, Monte Carlo simulations of a reactor-sized NCSX have found an α energy loss fraction of $F_{loss} \simeq 27\%$ after 6×10^4 toroidal transit times τ_ζ (roughly a slowing-down time).[2] Accordingly, to find an improved QA configuration for the ARIES-CS reactor study, Ku began from the LI383 design which is the basis for NCSX, and using the Stellopt optimizer[3], found a new configuration, N3ARE,[2] closely related to LI383, but in which F_{loss} was reduced to below 10%. Additionally, its thermal confinement was also substantially improved, with its "$1/\nu$" transport coefficient $D_{-1} \propto \epsilon_{ef}^{3/2}$ down from that of LI383 by a factor of roughly 5–8 over much of the minor radius, while other needed properties, such as MHD stability and equilibrium quality, were comparable to those in LI383. (Here, ϵ_{ef} is the "effective ripple strength"[4] of a given flux surface in a configuration.) Optimizers are very important design tools, but why they reach the solutions they do is often physically obscure. Our objective here is to enhance that physical understanding, which in turn facilitates the search for desirable configurations.

In Figs. 1 are shown the largest nonaxisymmetric ($n \neq 0$) Fourier amplitudes B_{mn} for (a)LI383 and (b)N3ARE versus $s \equiv \psi/\psi_a$, where $2\pi\psi$ is the toroidal flux on a given flux surface, and ψ_a is ψ at the edge. The 2 dominant B_{mn} in LI383 are B_{23} and B_{36}, of comparable size and opposite sign. In N3ARE these are substantially reduced

in magnitude, replaced by a dominant "mirror term" B_{03} and a sideband B_{13}, of size comparable to B_{23} and B_{36} in LI383.

The principal transport figure of merit (f.o.m.) used in obtaining LI383 is the QA measure $F_{Bmn} \equiv \langle \sum_{m,n \neq 0} B_{mn}^2 / B_{00}^2 \rangle_s$, where $\langle .. \rangle_s$ denotes a weighted average over flux surfaces s. To improve the α-confinement, Stellopt was run from LI383, replacing F_{Bmn} with F_{loss} (with a short run-time of a few hundred τ_ζ, for speed), and it was observed that B_{03} and B_{13}, suppressed by F_{Bmn}, had become appreciable. Accordingly, Stellopt was run further, instead using F'_{Bmn}, defined the same as F_{Bmn}, but with these $(m, n) = (0, 3), (1, 3)$ harmonics removed. N3ARE was then obtained by further evolution using ϵ_{ef} as the transport f.o.m., and then again using F_{loss}.

In Fig. 2a is a contour plot $B(s, \theta, \zeta)$ over a flux surface for LI383 for $s = 0.5$, with $\theta(\zeta)$ the poloidal (toroidal) azimuth in flux coordinates. The slanted straight line shows the magnetic field direction $\hat{\mathbf{B}}$. In Fig. 2b is plotted the profile $B(\ell)$ along a field line for one poloidal transit. In Figs. 3 are the analogous plots for N3ARE. The contours $B = \mathrm{const}$ in Figs. 2a and 3a run approximately in the ζ-direction, as one expects for a QA device. However, for each of its 3 field periods, in LI383 there is a marked inflection of the contours, bending first strongly to the left as one moves along a contour (indicated by the dashed ovals), and then more gently back to the right. The left bend has the effect of creating ripple wells on the slopes of the toroidal variation *i.e.*, around $\theta = \pi/2, 3\pi/2$ (*e.g.*, point a in Fig. 2b), as well as enhancing the gradient in B perpendicular to $\hat{\mathbf{B}}$, thereby increasing the radial drift velocity $\dot{\psi} \propto \hat{\mathbf{B}} \times \nabla B$ there. A weaker bend to the left is also visible for N3ARE in Fig. 3a, creating smaller ripple wells, or only a flattening of the toroidal slope in Fig. 3b.

One also sees a large ripple well in both configurations on the inboard side ($\theta \sim \pi$), deeper than those on the toroidal slopes, and much deeper for N3ARE than for LI383.

However, as one notes from the much improved confinement of N3ARE over LI383, these large wells are fairly benign, while the much smaller well at a in Fig. 3a provides a major additional loss channel in LI383, as will be seen.

In Figs. 4 are contour plots over a flux surface of $\dot{\psi}$ for the 2 configurations. From these alone, one might expect the confinement of N3ARE to be enhanced over that of LI383 only modestly. Both show peak ridges in $|\dot{\psi}|$ around $\theta = \pi/2, 3\pi/2$, the same θ-values for which the toroidal contribution ($\sim v_B \sin\theta$) peaks, enhanced by an additional helical contribution. The root mean square value $\dot{\psi}_{rms} \equiv \langle \dot{\psi}^2 \rangle^{1/2}$ of $\dot{\psi}$ for N3ARE is a little below (about 70%) that for LI383, which, assuming diffusion coefficient $D \sim \dot{\psi}_{rms}^2$, would predict a ratio $D^{N3ARE}/D^{LI383} \simeq 1/2$. (Here $\langle ... \rangle$ denotes a flux surface average.) The $\dot{\psi}$ peaks $\dot{\psi}_{mx}$ for LI383 occur exactly where the dashed oval in Fig. 2a is, manifesting the enhanced B-gradient arising from the strong inflection in the contour direction noted above. For N3ARE, the contour inflections are smaller, and more distributed, resulting in the modestly smaller, multiple peaks in $\dot{\psi}$.

However, a better indicator of a particle's rate of radial progress is not $\dot{\psi}$, but the bounce–averaged value $\bar{\dot{\psi}}$ of $\dot{\psi}$. $\bar{\dot{\psi}}(\theta, \zeta)$ is plotted in Fig. 5a for LI383 and in 5b for N3ARE, computed by taking $v_\parallel = 0$ for the particle at the plotted point, finding its other turning point along a field line, and then computing the bounce average between the 2 points using conservation of energy E and magnetic moment μ. One notes that the peak values $\bar{\dot{\psi}}_{mx}$ of $|\bar{\dot{\psi}}|$ fall almost exactly on those of $\dot{\psi}_{mx}$ for LI383, and they are of almost the same magnitude. In contrast, for N3ARE the peaks in $\bar{\dot{\psi}}$ occur closer to $\theta = 0, 2\pi$ than those of $\dot{\psi}$, where $\dot{\psi} \sim \sin\theta$ is smaller. Moreover, while $\dot{\psi}$ has 3 peaks per field period, $\bar{\dot{\psi}}$ exhibits only 1, with ζ-value near that of the rightmost of the 3 $\dot{\psi}$ peaks, making the region over which the peaks are appreciable much smaller than

for LI383. Thus, from these additional 2 factors, while $\langle \dot{\psi}^2 \rangle^{N3ARE} / \langle \dot{\psi}^2 \rangle^{LI383} \simeq 0.5$, as noted, one has $\langle \bar{\dot{\psi}}^2 \rangle^{N3ARE} / \langle \bar{\dot{\psi}}^2 \rangle^{LI383} \simeq 0.10$, comparable to the expected ratio $D_{-1}^{N3ARE} / D_{-1}^{LI383} \simeq 0.12$ at $s = 0.5$.

This further reduction can be understood by examining more closely the bounce-averaging yielding these $\bar{\dot{\psi}}$ values. The B-contour inflection in Fig. 2a is strong enough to produce a ripple well (labeled a) on the toroidal slope (around $\pi/2, 3\pi/2$). Thus, ripple-trapped particles here have a $\dot{\psi}$-value near $\dot{\psi}_{mx}$ over the full bounce, and so have $\bar{\dot{\psi}} \simeq \bar{\dot{\psi}}_{mx} \simeq \dot{\psi}_{mx}$ there. In contrast, in N3ARE the inflection producing $\dot{\psi}_{mx}$ is not large enough to produce a ripple well there – such wells only occur further down the toroidal slope, *i.e.*, toward $\theta = 0, 2\pi$, where the slope is smaller. Particles with a turning point around $\dot{\psi}_{mx}$ are thus toroidally-trapped, not ripple-trapped, so their $\bar{\dot{\psi}}$ is much smaller, both because they pass through a much larger range of θ, where $|\dot{\psi}|$ is smaller, and also because they average over regions of opposite signs of $\dot{\psi}$. And on the other hand, particles with turning points inside the ripple wells average over smaller $\dot{\psi}$ values there. These effects yield the further reduction of roughly 1/5 noted above.

Particles in the much deeper ripple-wells around $\theta = \pi$ in both devices also manifest very small values of $\bar{\dot{\psi}}$ in Fig. 5, for reasons similar to those described for toroidally-trapped particles.

The ripple wells on the toroidal slopes of LI383 act as "holes" in the magnetic bottle, providing a substantial new loss channel for particles to escape. A comparison of the typical α-loss orbits from LI383 and N3ARE bear this out. Many of the loss orbits in LI383 are particles initially toroidally-trapped, which become ripple-trapped in the $\bar{\dot{\psi}}_{mx}$ ripple near the bottom of the machine ($\theta \sim 3\pi/2$), and then drift nearly vertically out. Such loss orbits are very rare in N3ARE, for which toroidally-trapped particles tend to remain so, therefore making their way to the edge only via the much

slower drift of their banana-centers.

Thus, the general principles emerge that (1)ripple wells alone are not necessarily dangerous for QA confinement, but ripple wells on the toroidal slope are, and (2)strong "left-inflections" in the $B(\theta, \zeta)$ contours of a configuration tend to produce such wells, and so should be minimized.

As a further test of these rules, in Fig. 6 are displayed (a)$B(\theta, \zeta)$ and (b)$B(\ell)$ for a related third QA configuration, T8G. In contrast to N3ARE, T8G was produced with the same modular coil set used to produce LI383, and then optimized using a weighted combination of F'_{Bmn}, F_{loss}, and ϵ_{ef} for a transport f.o.m., allowing only the currents in the modular coils to vary. Such an optimization considerably constrains the range of configuration shapes available, and thus one might expect T8G's characteristics to fall between those of LI383 and N3ARE. Such an expectation is borne out by a number of device characteristics. The $n \neq 0$ B_{mn}-spectrum and the $B(\theta, \zeta)$ plot of T8G look like hybrids of those for LI383 and N3ARE. The $B(\ell)$ profile of T8G bears some resemblance to that of LI383, but has developed the 2 large peaks around $\theta = \pi$ exhibited by N3ARE, and the ripple-well a in Fig. 2a for LI383 has been reduced in size. ϵ_{ef} for T8G lies between those of LI383 and N3ARE, as are its α-loss fractions. At the edge, ϵ_{ef} has values 1.7, 0.82, and 0.57 % for LI383, T8G, and N3ARE, respectively, maintaining this ordering inward to $s \sim 0.3$. And in the same ordering, F_{loss} for $300\tau_{\zeta}$ equals 15, 10, and 4.5 %, resp. The $B(\ell)$ profile of T8G is considerably less smooth than that for LI383, with more ripple wells, so that one might naively expect it to have worse transport than LI383. In fact, however, consistent with rule (1) above, its confinement is significantly better – the wells at problematic θ values are smaller, and the extra ripple wells occur away from those problematic θ values.

For purposes of numerically implementing these design rules, some of the vari-

ous f.o.m.s which have been used for improving stellarator transport already capture them. The "numerical" f.o.m.s, *i.e.*, those based on numerical integration of an ensemble of orbits, capture them, essentially by definition. This includes F_{loss} for energetic confinement, and standard Monte-Carlo computations of thermal diffusion coefficient D. The numerical f.o.m.s, however, suffer from the difficulty of having long evaluation times, and/or statistical noisiness, which interfere with an optimizer's operation. As expected, D bears out the predictions of the f.o.m.s ϵ_{ef} or $D_{-1} \propto \epsilon_{ef}^{3/2}$. The latter f.o.m.s are of the "semi-analytic" type, *i.e.*, theory-based expressions which are then typically evaluated computationally for any given configuration. Another semi-analytic f.o.m. discussed here, similar to but simpler than D_{-1} or ϵ_{ef}, is the flux-surface average $\langle \bar{\dot{\psi}}^2 \rangle$, which also correlates well with the numerical f.o.m.s. Others of this class, *e.g.*, F_{Bmn} or the "water measure" W,[5] do not capture these rules, the former since it discriminates against all B_{mn} equally, as noted, and the latter since it would weigh (*e.g.*) the large ripple wells around $\theta = \pi$ as much more problematic than the small wells around $\theta = \pi/2, 3\pi/2$.

All of the semi-analytic f.o.m.s mentioned above are radially local, *i.e.*, they are evaluated on a given flux surface ψ. Thus, they miss the "radial connectivity" necessary for energetic ion loss. That is, a particle which drifts readily across one flux surface can still be well-confined if it drifts to another surface where $\bar{\dot{\psi}}$ becomes small, *e.g.*, by the ripple well it is trapped in vanishing as one moves radially outward. Such connectivity is present in the QAs examined here. However, configurations might be found in which this is not the case, and for these, the radially local f.o.m.s would provide overly pessimistic expectations. One semi-analytic f.o.m. which is radially nonlocal seeks to make contours of the second adiabatic invariant J a function of ψ alone.[6]. However, such a f.o.m. is not useful for QAs — in QAs, ripple trapped parti-

cles must drift almost vertically, and therefore making $J \simeq J(\psi)$ is not possible.

Regarding NCSX in particular, as suggested by the discussion here, it should be possible to create T8G in that machine as well as the standard LI383 configuration just by varying the currents in its modular coil set, and thereby to partially plug the holes in LI383. Moreover, an additional set of trim coils is being designed with which it should be possible to create N3ARE, or some approximation, to further improve upon neoclassical confinement.

Acknowledgment

[1] G.H. Neilson, M.C. Zarnstorff, J.F. Lyon, the NCSX Team, *Journal of Plasma and Fusion Research* **78**, 214-219 (2002).

[2] L.P. Ku, P. Garabedian, *Proceedings 15th International Stellarator Workshop*, (Madrid, Spain, 2005) (to appear in *Fusion Science and Technology*, 2006).

[3] A. Reiman, G. Fu, S. Hirshman, L. Ku, *et al.*, *Plasma Phys. Control. Fusion* **41** B273 (1999).

[4] V.V. Nemov, S.V. Kasilov, W. Kernbichler, M.F. Heyn, *Phys.Plasmas* **6**, 4622 (1999).

[5] M.Yu. Isaev, M.I. Mikhailov, D.A. Monticello, H.E. Mynick, A.A. Subbotin, L.P. Ku, A.H. Reiman, *Phys. Plasmas* **6**, 3174 (1999).

[6] S.P. Hirshman, D.A. Spong, J.C. Whitson, V.E. Lynch, D.B. Batchelor, B.A. Carreras, J.A. Rome, Phys. Rev. Letters **80**, 528 (1998).
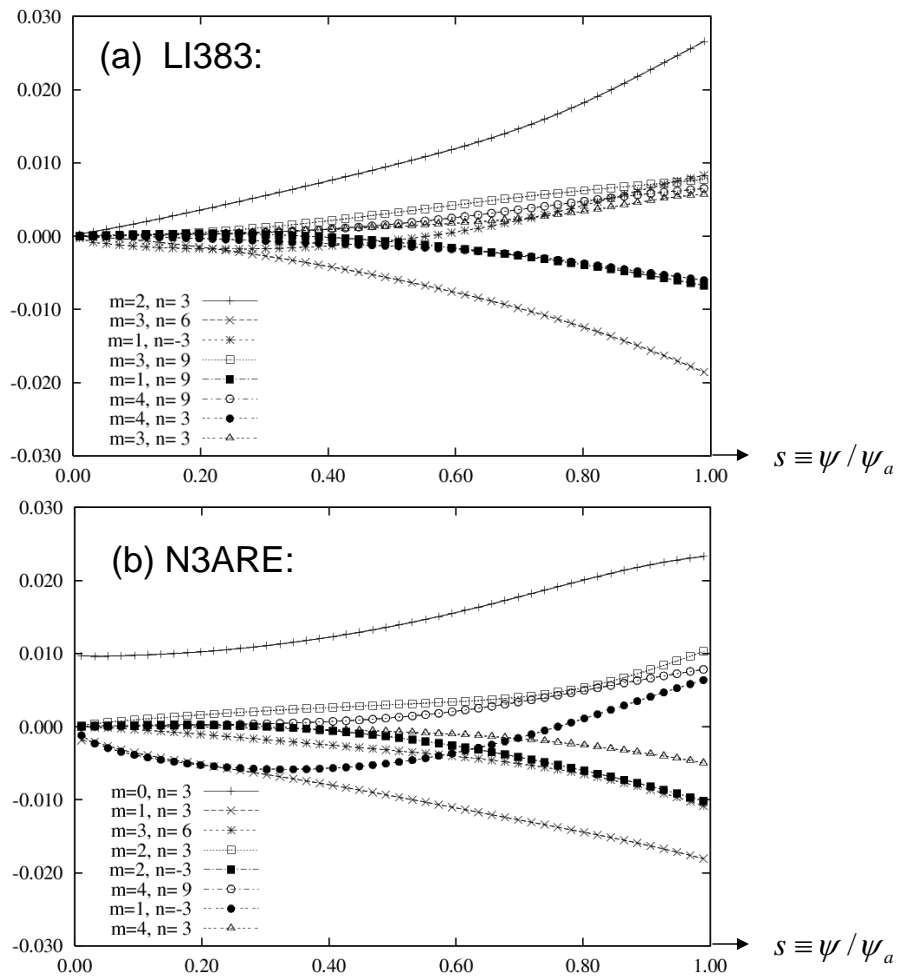
FIG. 1: Dominant nonaxisymmetric Fourier amplitudes B_{mn} for (a)LI383 and (b)N3ARE, versus normalized toroidal flux s.
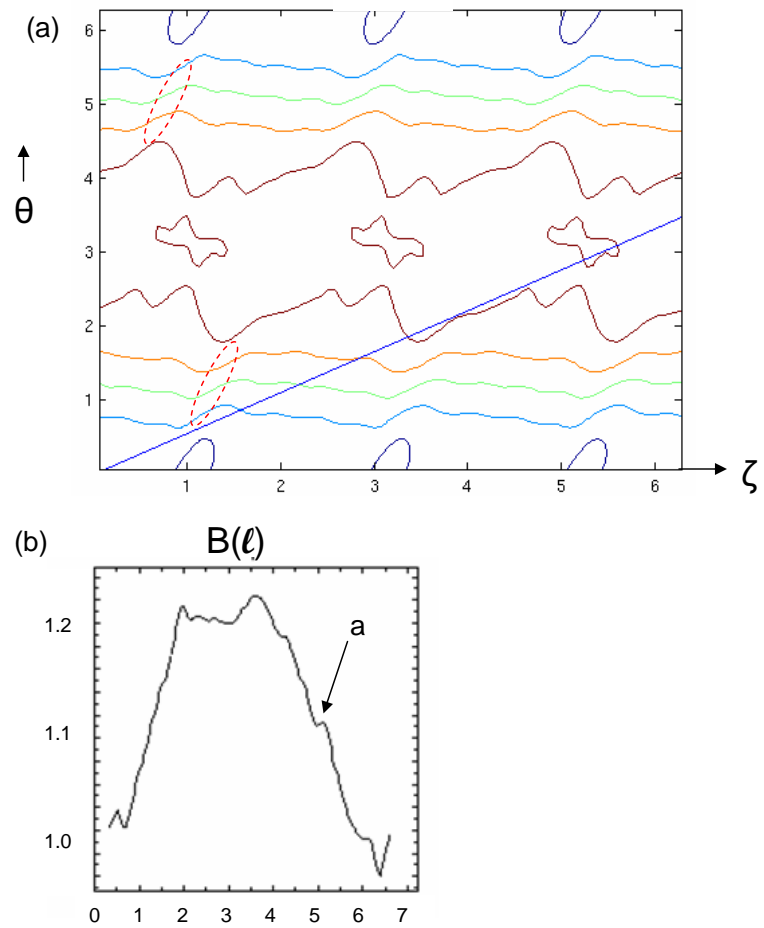
FIG. 2: (a)Contour plot of $B(s = 0.5, \theta, \zeta)$ over a flux surface and (b)profile $B(\ell)$ along a field line for one poloidal transit, for LI383.

(a)

θ

ζ

B(ℓ)

(b)
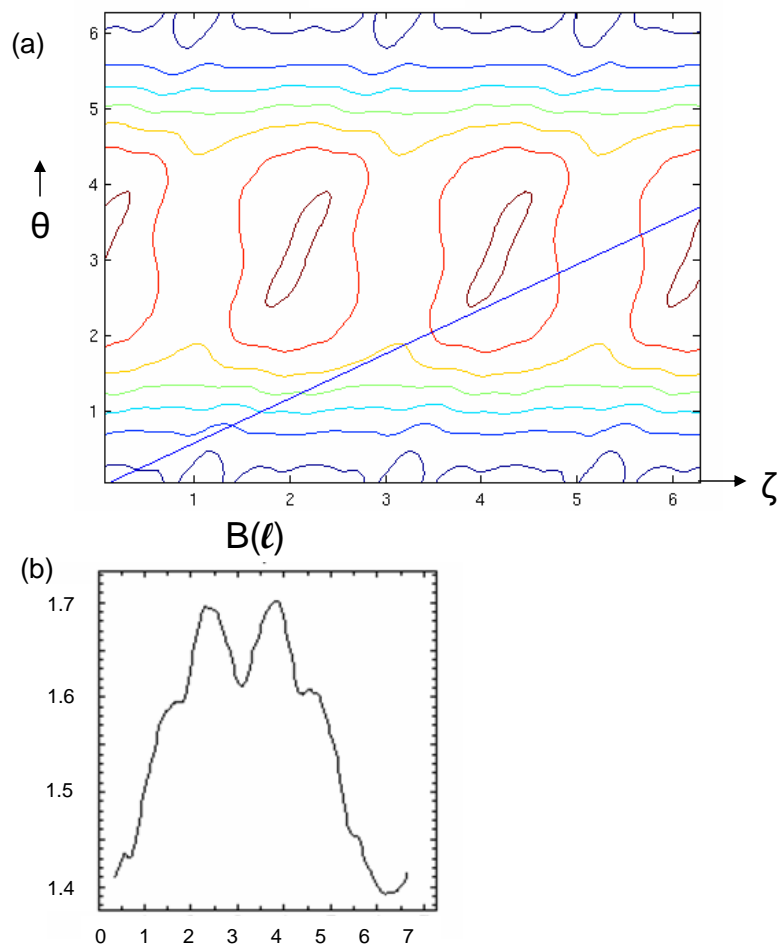
FIG. 3: Analogous plots to Figs. 2, but for N3ARE.
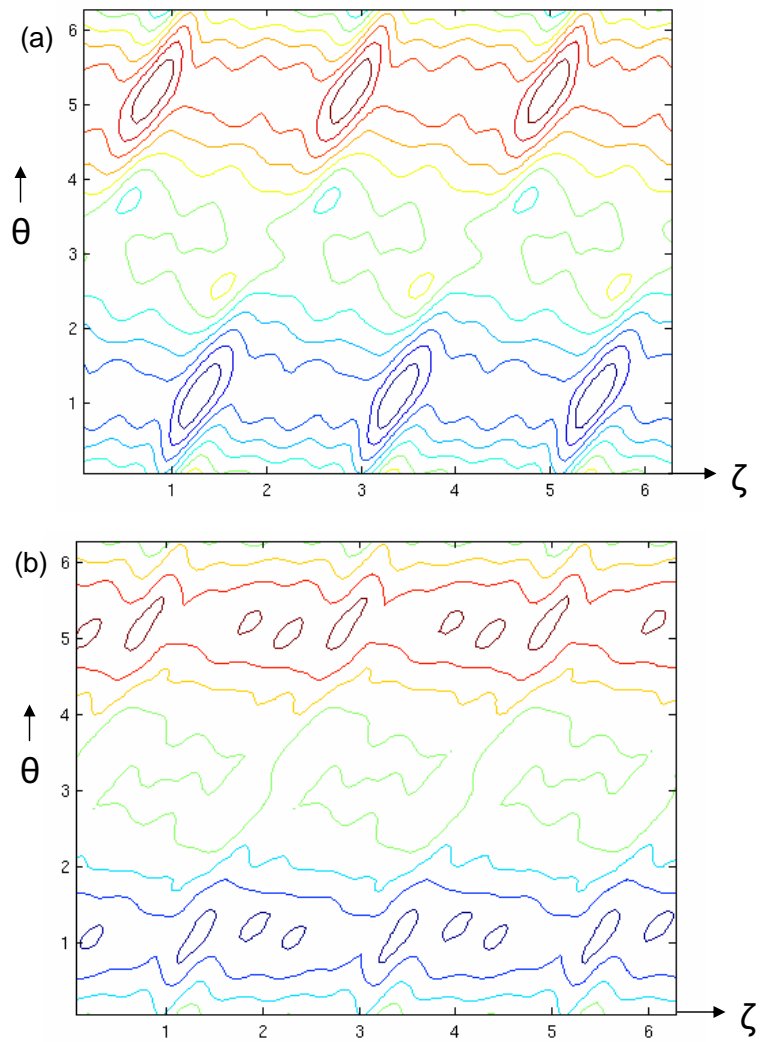
FIG. 4: $\dot{\psi}$ over a flux surface for (a)LI383 and (b)N3ARE, for $s = 0.5$.
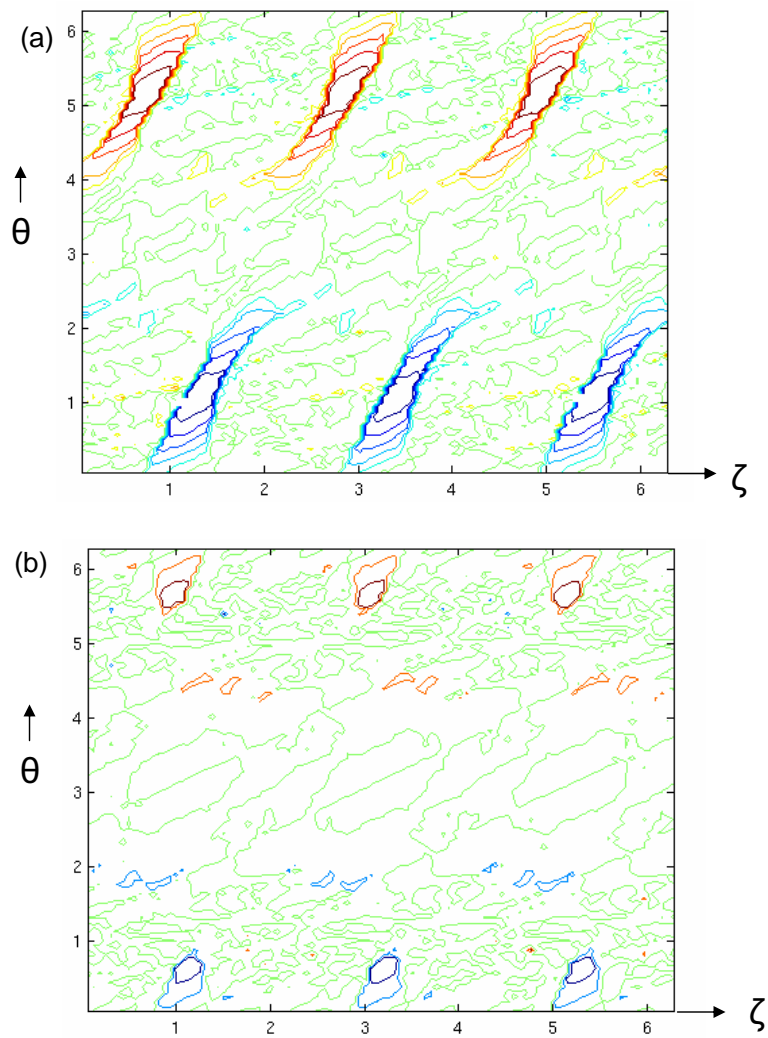
FIG. 5: $\bar{\bar{\psi}}$ over a flux surface for (a)LI383 and (b)N3ARE, for $s = 0.5$.

(a)

(b)

B(ℓ)
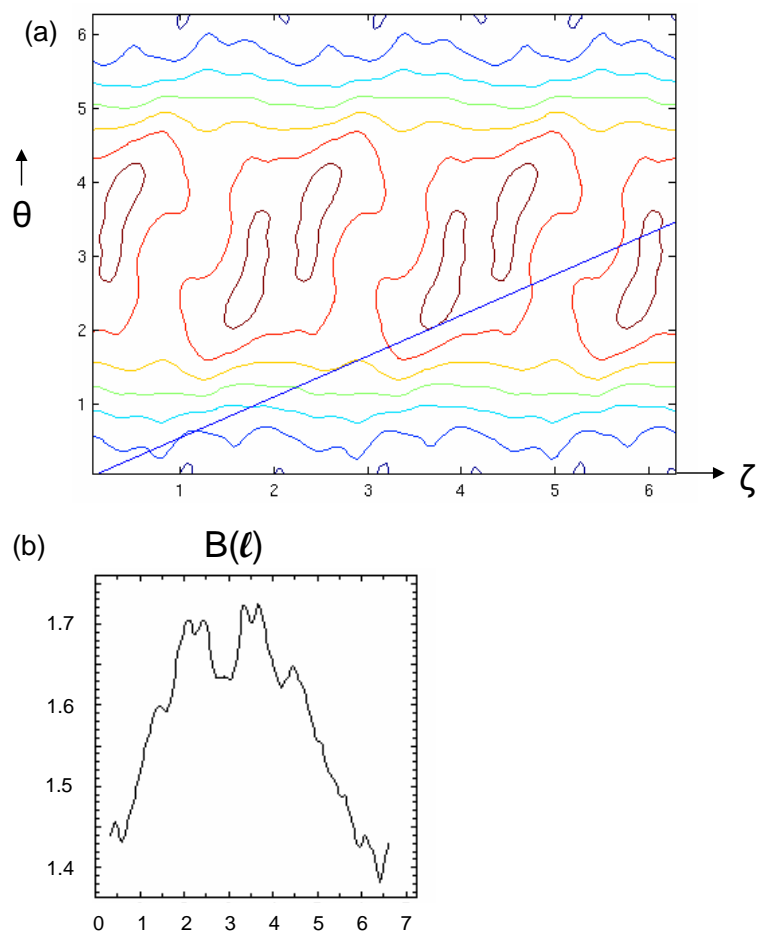
FIG. 6: Analogous plots to Figs. 2, 3, but for T8G.

External Distribution

Plasma Research Laboratory, Australian National University, Australia

Professor I.R. Jones, Flinders University, Australia

Professor João Canalle, Instituto de Fisica DEQ/IF - UERJ, Brazil

Mr. Gerson O. Ludwig, Instituto Nacional de Pesquisas, Brazil

Dr. P.H. Sakanaka, Instituto Fisica, Brazil

The Librarian, Culham Science Center, England

Mrs. S.A. Hutchinson, JET Library, England

Professor M.N. Bussac, Ecole Polytechnique, France

Librarian, Max-Planck-Institut für Plasmaphysik, Germany

Jolan Moldvai, Reports Library, Hungarian Academy of Sciences, Central Research
    Institute for Physics, Hungary

Dr. P. Kaw, Institute for Plasma Research, India

Ms. P.J. Pathak, Librarian, Institute for Plasma Research, India

Dr. Pandji Triadyaksa, Fakultas MIPA Universitas Diponegoro, Indonesia

Professor Sami Cuperman, Plasma Physics Group, Tel Aviv University, Israel

Ms. Clelia De Palo, Associazione EURATOM-ENEA, Italy

Dr. G. Grosso, Instituto di Fisica del Plasma, Italy

Librarian, Naka Fusion Research Establishment, JAERI, Japan

Library, Laboratory for Complex Energy Processes, Institute for Advanced Study,
    Kyoto University, Japan

Research Information Center, National Institute for Fusion Science, Japan

Professor Toshitaka Idehara, Director, Research Center for Development of Far-Infrared Region,
    Fukui University, Japan

Dr. O. Mitarai, Kyushu Tokai University, Japan

Mr. Adefila Olumide, Ilorin, Kwara State, Nigeria

Dr. Jiangang Li, Institute of Plasma Physics, Chinese Academy of Sciences, People's Republic of China

Professor Yuping Huo, School of Physical Science and Technology, People's Republic of China

Library, Academia Sinica, Institute of Plasma Physics, People's Republic of China

Librarian, Institute of Physics, Chinese Academy of Sciences, People's Republic of China

Dr. S. Mirnov, TRINITI, Troitsk, Russian Federation, Russia

Dr. V.S. Strelkov, Kurchatov Institute, Russian Federation, Russia

Kazi Firoz, UPJS, Kosice, Slovakia

Professor Peter Lukac, Katedra Fyziky Plazmy MFF UK, Mlynska dolina F-2, Komenskeho Univerzita,
    SK-842 15 Bratislava, Slovakia

Dr. G.S. Lee, Korea Basic Science Institute, South Korea

Dr. Rasulkhozha S. Sharafiddinov, Theoretical Physics Division, Insitute of Nuclear Physics, Uzbekistan

Institute for Plasma Research, University of Maryland, USA

Librarian, Fusion Energy Division, Oak Ridge National Laboratory, USA

Librarian, Institute of Fusion Studies, University of Texas, USA

Librarian, Magnetic Fusion Program, Lawrence Livermore National Laboratory, USA

Library, General Atomics, USA

Plasma Physics Group, Fusion Energy Research Program, University of California at San Diego, USA

Plasma Physics Library, Columbia University, USA

Alkesh Punjabi, Center for Fusion Research and Training, Hampton University, USA

Dr. W.M. Stacey, Fusion Research Center, Georgia Institute of Technology, USA

Director, Research Division, OFES, Washington, D.C. 20585-1290